

# LINA: Linear Autoregressive Image Generative Models with Continuous Tokens

Jiahao Wang<sup>1</sup> Ting Pan<sup>2</sup> Haoge Deng<sup>2</sup> Dongchen Han<sup>3</sup> Taiqiang Wu<sup>1</sup> Xinlong Wang<sup>4</sup> Ping Luo<sup>1</sup>

## Abstract

Autoregressive models with continuous tokens represent a unique paradigm for visual generation, showing strong promise in text-to-image (T2I) synthesis but suffering from heavy computational costs. In this work, we investigate how compute-efficient linear attention should be designed within this framework. We start with a systematic empirical study to examine how linear attention scales with parameter counts under different design choices. Specifically, we examine two key design choices: (i) *normalization paradigms* in linear attention—division-based *vs.* subtraction-based, and (ii) the use of a *depthwise convolution* on image features for locality modeling augmentation. The scaling results indicate that while subtraction-based normalization is effective for image classification, division-based normalization is more amenable to linear generative transformers; besides, convolutions play a key role in linear attention for autoregressive modeling, consistent with prior findings in diffusion models. Furthermore, we explore introducing *gating mechanisms*, a key design choice in causal linear attention, into bidirectional linear attention, and as a result, we propose a *KV gate*. By applying data-independent learnable parameters to the key and value states, our method assigns token-wise weights to memory, enabling flexible memory management, similar to the forget gate in language models. Building on these designs, we offer LINA, a simple and compute-efficient text-to-image generative model with pure linear attention, capable of rapidly generating high fidelity  $1024 \times 1024$  images from user instructions. LINA achieves strong results on both class-conditional and T2I generation. Compared to diffusion models of similar scale and autoregressive models with softmax attention, LINA delivers competitive

performance—FID of 2.18 on ImageNet ( $\sim 1.4B$ ) and an overall score of 0.74 on GenEval ( $\sim 1.5B$ ). For efficiency, a single linear attention module reducing FLOPs by  $\sim 61\%$  over softmax attention. Code and models are released at <https://github.com/techmonsterwang/LINA>.

## 1. Introduction

The field of image generation is evolving rapidly (Ho et al., 2020; Peebles & Xie, 2023; Chen et al., 2024b;a). Autoregressive models with continuous tokens (Li et al., 2024b) emerge as a competitive alternative to diffusion models and show strong promise, having been validated in text-to-image tasks (Fan et al., 2025a), inspiring video generation (Deng et al., 2025), and scaling up to large models (*e.g.*, 14B parameters (Team et al., 2025)). The paradigm involves both multi-step autoregression and diffusion, and a major bottleneck lies in its efficiency: its reliance on quadratic computation complexity softmax attention (Vaswani et al., 2017) makes it less practical for long-sequence generation such as high-resolution images or long videos.

Linear attention (Katharopoulos et al., 2020), as a natural alternative, has been extensively explored in both vision transformer (ViT) (Dosovitskiy et al., 2020)-based perception models (Cai et al., 2023; Han et al., 2023) and diffusion transformer (DiT) (Peebles & Xie, 2023)-based generative models (Xie et al., 2025a;b; Wang et al., 2025). However, it remains unclear how linear attention should be adapted to autoregressive generative models. Unlike DiTs, which generate tokens in parallel, autoregressive models perform inference in a sequential manner: image tokens are generated step by step, with the set of known tokens gradually expanding as the inference progresses. Such distinction suggest that the design choices for linear attention may need a careful reconsideration, *e.g.*, normalization paradigms (Han et al., 2024), and gating mechanisms (Yang et al., 2024; 2025) commonly used in autoregressive language models.

In this paper, we systematically study what suitable design choices of linear attention fit autoregressive image generative models. Our approach builds on the NOVA (Deng et al., 2025) framework as the baseline, and we analyze linear-attention design choices for ImageNet (Deng et al., 2009)

<sup>1</sup>The University of Hong Kong <sup>2</sup>University of Chinese Academy of Sciences <sup>3</sup>Tsinghua University <sup>4</sup>Beijing Academy of Artificial Intelligence. Correspondence to: Xinlong Wang <[wangxinlong@baai.ac.cn](mailto:wangxinlong@baai.ac.cn)>, Ping Luo <[pluo@cs.hku.hk](mailto:pluo@cs.hku.hk)>.



Figure 1. Qualitative results of 1024px samples powered by LINA.

$256 \times 256$  class-conditional image (C2I) generation. To start with, we conduct an empirical study on the *scaling behavior w.r.t. parameter counts*, focusing on two main factors: *normalization paradigm* and *locality augmentation* of linear attention (Sec. 4). The underlying reason is straightforward. Normalization enforces the attention weights to sum to one, which stabilizes the scale of activations and influences training dynamics. Meanwhile, linear attention, compared with softmax attention, is well known to suffer from insufficient locality modeling (Han et al., 2023; 2024). Thus, we introduce two design choices: division-based versus subtraction-based normalization for linear attention, and whether image tokens should be augmented with locality. For each setting, we train models at three model capacities:  $\sim 0.4\text{B}$ ,  $\sim 0.6\text{B}$ , and  $\sim 1.4\text{B}$  parameters. Counterintuitively, the injectivity brought by subtraction-based normalization turns out to be *not* essential for autoregressive image generative modeling, despite its emphasized role in classification models (Han et al., 2024). Meanwhile, the inductive bias (Cordonnier et al., 2019) introduced by depthwise convolution (DWC) for locality enhancement does *not* appear to be restrictive when scaling up parameters.

Then, we explore the gating mechanism (Yang et al., 2024; 2025; Zhang et al., 2024; Lin et al., 2025; Qiu et al., 2025)—commonly used in autoregressive language models—for image generative modeling (Sec. 5). In prior work, gating has been shown to flexibly manage the memory in *causal* linear attention. However, a key challenge is how to adapt it to the *bidirectional* attention used in image generation, where we develop a simple yet effective *KV gate* method. KV gate are *data-independent*, scalar-valued *learnable parameters* with *no* explicit range constraints. By applying independent gating factors to the key and value, they enable flexible memory management and fits naturally with bidirectional attention. We conduct detailed ablation studies on their different modes and find that proper management

of *both the memory and the normalization term* is crucial. We further provide detailed visualizations of the KV gate to see what it has learned.

Lastly, based on these explorations, we propose LINA, a compute-efficient linear autoregressive image generative model (Sec. 6). LINA employs *division-based normalization* linear attention enhanced with a *DWC module* for locality enhancement, together with the *KV gate*. We first validate LINA on class-conditional image generation, achieving an FID of 2.18 on the ImageNet  $256 \times 256$  benchmark, which is competitive with SOTA diffusion models. We further extend LINA to text-to-image generation, where it follows user instructions and efficiently produces high-fidelity images up to 1024px, achieving a highly competitive GenEval score of 74. In terms of efficiency, linear attention in our LINA reduces FLOPs by  $\sim 61\%$  compared with softmax attention when generating 1024px images, demonstrating the computational advantage of our approach.

Through LINA, we seek to unlock the potential of linear attention and call on the community to develop efficient transformer alternatives for broad applications.

## 2. Related Work

Here we briefly review related work. A detailed version is provided in Appendix A. Our study builds on autoregressive models with continuous tokens (Li et al., 2024b; Fan et al., 2025a), which have become a mainstream approach in image generation in recent years. This line of research has been explored not only with 14B-parameter autoregressive models (e.g., NextStep-1 (Team et al., 2025)), but also successfully extended to video generation (e.g., NOVA (Deng et al., 2025)). One of the key bottlenecks of such methods lies in their computational efficiency. To this end, we draw inspiration from efficient linear attention (Katharopoulos et al., 2020; Choromanski et al., 2021), which has already

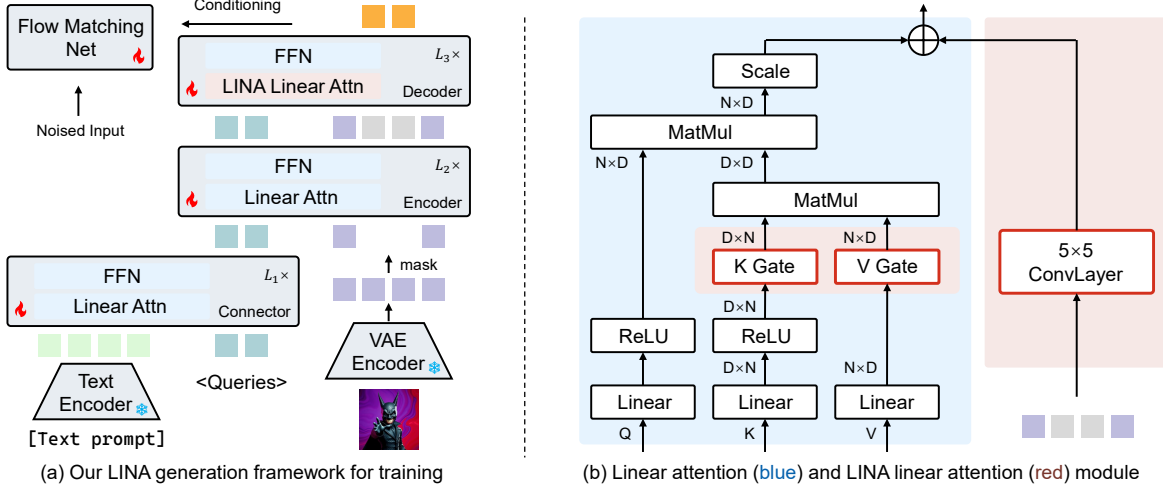


**Figure 2. Overview of LINA:** Fig. (a) illustrates the training pipeline, with a *Connector* for extracting text information, an *Encoder* to extract unmasked tokens, and a *Decoder* to reconstruct masked tokens for conditioning. A denoising flow matching MLP is used to sample tokens. Fig. (b) shows the *division-based normalization* linear attention, and our introduced DWC module and KV gate (Sec. ??).

been successfully applied to both LLMs (Yang et al., 2024) and visual perception task (Cai et al., 2023; Han et al., 2023). Along this line, several studies (Xie et al., 2025a;b; Wang et al., 2025; Zhu et al., 2024; Pu et al., 2024) have studied designing efficient DiTs with linear attention. Differently, we thoroughly discuss how linear attention should be designed in autoregressive image generative models.

### 3. Preliminary

#### 3.1. Autoregressive Modeling with Continuous Tokens

Given a target of  $N$  tokens  $\{X_1, \dots, X_N\}$  to predict, masked autoregressive models (MAR) (Li et al., 2024b) complete the prediction task in  $K$  steps. Illustrated in Fig. 2-(a), at every step  $k$ , a random-order autoregressive model predicts a set of tokens  $\mathbf{S}_k = \{X_i, X_{i+1}, \dots, X_j\}$  with  $\cup_k \mathbf{S}_k = \{X_1, \dots, X_N\}$ , conditioned on the previously generated tokens  $\{X_1, \dots, X_{i-1}\}$ :

$$\begin{aligned} p(X_1, \dots, X_N) &= p(\mathbf{S}_1, \dots, \mathbf{S}_K) \\ &= \prod_k^K p(\mathbf{S}_k \mid \mathbf{S}_1, \dots, \mathbf{S}_{k-1}). \end{aligned} \quad (1)$$

Typically, MAR models consist of a network (e.g., Transformer (Vaswani et al., 2017)) that predicts a condition vector from the input, and a diffusion (Ho et al., 2020; Sohl-Dickstein et al., 2015) or flow matching (Lipman et al., 2023; Liu et al., 2023) head (e.g., MLP) that models the next token distribution conditioned on this vector.

Efficiency is a practical challenge for MAR framework, as both the autoregressive and diffusion processes require multiple iterations. In this work, we take a closer look at the design choices of linear attention in this context, focusing

on scaling behavior with parameter and gating mechanisms.

#### 3.2. Linear Attention

Given an input sequence  $I \in \mathbb{R}^{N \times D}$  of length  $N$ , we denote the queries, keys, and values in linear attention (Katharopoulos et al., 2020) by  $Q, K, V \in \mathbb{R}^{N \times D}$ . We refer to the kernel function as  $\phi(\cdot)$  (e.g., ReLU) and the output as  $O \in \mathbb{R}^{N \times D}$  (for simplicity, we assume attention head as 1). Linear attention introduces a normalization factor  $\gamma \in \mathbb{R}^N$  that ensures the normalized attention weights for each token  $i$  sum to 1. Based on how this normalization term is defined, we categorize linear attention as follows<sup>1</sup>.

**Division-based normalization.** In this formulation, the normalization factor in linear attention is placed in the denominator, akin to the softmax operation in full attention (Vaswani et al., 2017):

$$\begin{aligned} O_i^{(d)} &= \sum_{j=1}^N \frac{A_{ij}^{(d)}}{\gamma_i^{(d)}} V_j = \sum_{j=1}^N \frac{\phi(Q_i) \phi(K_j)^\top}{\sum_{m=1}^N \phi(Q_i) \phi(K_m)^\top} V_j \\ &= \frac{\phi(Q_i) \left( \sum_{j=1}^N \phi(K_j)^\top V_j \right)}{\phi(Q_i) \left( \sum_{m=1}^N \phi(K_m)^\top \right)}, \end{aligned} \quad (2)$$

where  $\gamma_i^{(d)} \in \mathbb{R}$  denotes the scalar-valued division-based normalization term, calculated from  $Q_i \in \mathbb{R}^{1 \times D}$  and the set of key states  $K_m \in \mathbb{R}^{1 \times D}$  for  $m \in [1, N]$ . Linear attention reduces the computational complexity from  $\mathcal{O}(N^2)$  in full attention to  $\mathcal{O}(N)$ , since for every query  $Q_i$ ,

<sup>1</sup>Here our terminology is based on (Han et al., 2024) and (Fan et al., 2025b).

both the memory  $M = \sum_{j=1}^N \phi(K_j)^\top V_j \in \mathbb{R}^{D \times D}$  and  $z = \sum_{m=1}^N \phi(K_m)^\top \in \mathbb{R}^{D \times 1}$  are shared and thus need to be computed only once.

**Subtraction-based normalization.** In this form, the normalization term is introduced as a distinct term, imparting linear attention with an injective property (Han et al., 2024):

$$\begin{aligned} O_i^{(s)} &= \sum_{j=1}^N \left( A_{ij}^{(s)} - \gamma_i^{(s)} \right) V_j \\ &= \phi(Q_i) \left( \frac{1}{N} \sum_{j=1}^N \phi(K_j)^\top V_j \right) \\ &\quad - \left( \phi(Q_i) \frac{1}{N} \sum_{m=1}^N \phi(K_m)^\top - 1 \right) \frac{1}{N} \sum_{j=1}^N V_j, \end{aligned} \quad (3)$$

where  $\gamma_i^{(s)} \in \mathbb{R}$  denotes the scalar-valued subtraction-based normalization term. Injective property allows linear attention (Eq. 3) to distinguish different queries, which is similar to softmax attention.

## 4. Scaling Behavior of Linear Attention

Despite linear attention has shown promise in DiTs (Pu et al., 2024; Xie et al., 2025a;b) and ViTs (Cai et al., 2023; Han et al., 2023; Guo et al., 2024), its suitable design for autoregressive image generation task remains unclear in the literature, inspiring us to find suitable design choices of linear attention to save computation while retaining generative performance. In this section, we focus on the scaling behavior with respect to parameter counts of linear attention and highlight two core design choices. **Q1 (linear attention paradigm choice):** Which paradigm—division-based or subtraction-based normalization—better supports parameter scaling? **Q2 (locality choice):** Without softmax, linear attention shows limited ability to model local patterns, which may affect performance. Does introducing a locality inductive bias affect parameter scaling?

To answer this question, we build our model upon the NOVA (Deng et al., 2025) framework, but rigorously replaces all softmax attention with linear attention. As shown in Fig. 2 (the inference framework are provided in Appendix B), the model consists of: a *Connector* for integrating text or class information; an *Encoder* and *Decoder* for predicting conditioning; and a denoising flow matching network (*i.e.*, a small MLP) (Li et al., 2024b) for modeling token probability distributions. We conduct a systematic scaling study to compare different linear attention paradigms and the effect of introducing a DWC module for locality modeling enhancement.

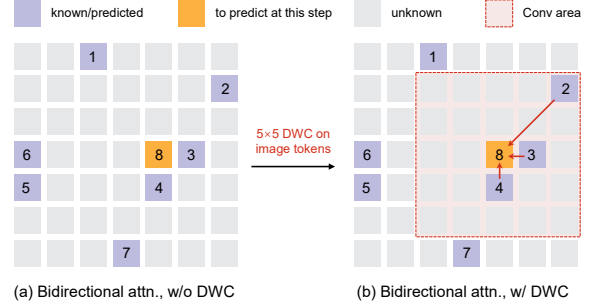


**Figure 3. DWC helps locality.** (a) A random-order autoregressive model with bidirectional attention predicts next tokens based on the predicted tokens (*e.g.*, the 8th). When the target token (*e.g.*, the 8th) is surrounded by predicted tokens (*e.g.*, the 3rd), the model faces challenges due to the limited local modeling capacity. (b) DWC module gathers information from nearby known tokens when predicting the current token, thereby facilitating linear attention.

### 4.1. Normalization Paradigm: Division vs. Subtraction

We empirically compare the scaling behaviors w.r.t. parameter counts of division-based and subtraction-based normalization linear attention (discussed in Sec. 3.2) in the context of autoregressive generative modeling, even though both forms have already been studied in diffusion modeling using DiTs (Peebles & Xie, 2023) or image classification via ViTs (Dosovitskiy et al., 2020; Touvron et al., 2021). We consider this comparison to be necessary. Unlike DiTs or ViTs, which generate all tokens in parallel, MAR models generate tokens sequentially in a step-by-step manner. At each step, they rely on previously predicted tokens to produce the next set. In the early stages of inference, only a few predicted tokens are available. Therefore, effectively exploiting the semantic context is vital for generation.

### 4.2. Locality Augmentation in Linear Attention

A key issue of linear attention is its capacity for local modeling (Han et al., 2023; 2024). Unlike softmax attention, it does not apply the `softmax` operation. Note that `Softmax` may account for the difference in locality modeling between softmax and linear attention.

$$\begin{aligned} H &= \begin{bmatrix} 5.0 & 1.0 & 0.5 \\ 0.5 & 4.0 & 1.0 \\ 1.0 & 0.5 & 3.5 \end{bmatrix}, \\ A^{(f)} &= \begin{bmatrix} 0.9714 & 0.0178 & 0.0108 \\ 0.0280 & 0.9259 & 0.0461 \\ 0.0725 & 0.0440 & 0.8835 \end{bmatrix} \approx \begin{bmatrix} 1 & 0 & 0 \\ 0 & 1 & 0 \\ 0 & 0 & 1 \end{bmatrix}. \end{aligned} \quad (4)$$

We provide a numerical example to clarify this effect. Consider a matrix  $H$  (Eq. 4). After applying `softmax`, the results  $A^{(f)} = \text{softmax}(H)$  becomes nearly identical to an identity matrix, implying that each token primarily attends to itself—representing the limiting case of local modeling.

In this case, although  $H$  may differ from the identity matrix, softmax helps sharpening the attention distribution, an essential operation that linear attention lacks. Thus, linear attention may face challenges in learning local relations.

**Does scaling MAR models benefit from locality augmentation? A conceptual discussion.** As shown in Fig. 3-(a), MAR models generate tokens set by set during inference. When the tokens to be predicted are adjacent to already known tokens, the latter provide valuable context, as neighboring tokens typically exhibit semantic correlations. We argue that, in this context, locality modeling is a crucial property in which linear attention is limited. As shown in Fig. 3-(b), we apply a  $5 \times 5$  *depthwise convolution* (DWC) (Chollet, 2017; Howard et al., 2017) module to potentially cooperate with linear attention, as its effectiveness has been extensively validated in both ViTs (Han et al., 2023; 2024) and DiTs (Wang et al., 2025). During inference, when predicting a token in an autoregressive step, DWC module incorporates neighboring predicted tokens (if available). If these known tokens are spatially close to the target token in 2D space, they tend to share similar semantics, providing useful cues for generation. On the other hand, pure ConvNets show limited scaling potential (e.g., ConvNeXt V2 (Liu et al., 2022; Woo et al., 2023) at  $\sim 650$ M parameters) compared with vision transformers (e.g., ViT-22B (Dehghani et al., 2023) at  $\sim 22$ B parameters). As a result, we ablate the use of DWC as a design choice to examine its effect on scaling behavior w.r.t. parameter counts.

**Implementation.** Unlike prior works (Han et al., 2023) that apply convolution to the value, we add DWC module to image features  $I_{\text{img}}$  *only* to the LINA *Decoder*—excluding the query features—and add its output to that of linear attention before the output projection of the attention:

$$\begin{aligned} O^{(d)} &= \text{LA}^{(d)}([I_q, I_{\text{img}}]) + \text{DWC}(I_{\text{img}}), \\ O^{(s)} &= \text{LA}^{(s)}([I_q, I_{\text{img}}]) + \text{DWC}(I_{\text{img}}), \end{aligned} \quad (5)$$

where  $\text{LA}^{(d)}$  and  $\text{LA}^{(s)}$  denote linear attention with division-based normalization and subtraction-based normalization, respectively. The reasons are twofold. First, query features  $I_q$  already incorporate textual conditioning, rendering the 2D inductive bias of DWC unnecessary. Second, LINA encoder inputs consist only of randomly predicted image tokens, where reshaping them into a 2D layout produces neighborhoods that are not equivalent to those formed by the full set of image features, limiting the benefit of DWC at this stage. With  $L_D$  decoder layers, DWC introduces only  $k \times k \times D \times L_D \approx 0.31$ M parameters, which is negligible compared with the overall model size of about 0.4B parameters.

### 4.3. Scaling Behaviors

**Experimental setup.** Based on the two design choices discussed above, we have four distinct settings. For each setting, we train models of three sizes, with  $\sim 0.4$ B,  $\sim 0.6$ B, and  $\sim 1.4$ B parameters, respectively. The evaluation is conducted on ImageNet (Deng et al., 2009) class-conditional image generation at  $256 \times 256$  resolution. All models are trained for 200K iterations on 32 A100 (40GB) GPUs with a learning rate of  $8 \times 10^{-4}$ . Inference is performed with BFloat16 precision. We report performance without classifier-free guidance (CFG) (Ho & Salimans, 2022), including FID-50K (Heusel et al., 2017), sFID (Nash et al., 2021), Inception Score (Salimans et al., 2016), and Precision/Recall (Kynkänniemi et al., 2019). Detailed model configuration, hyper-parameters and results are presented in Appendix C, D, and G, respectively.

**Division-based normalization empirically scales better than subtraction-based normalization.** Fig. 4-(a) illustrates the scaling performance of the four configurations, reported in terms of FID and IS. We observe that, regardless of the DWC module, division-based linear attention consistently outperforms subtraction-based at the huge scale ( $\sim 1.4$ B). We hypothesize two possible reasons: (1) semantic confusion (Han et al., 2024) may be absent in autoregressive image generation, or its impact is less pronounced than in vision perception models; and (2) at early generation steps, when few tokens are predicted, masked tokens may interfere more with subtraction-based normalization.

**DWC module tends to improve both linear attention variants across model sizes.** From Fig. 4-(b), we further observe that for both forms of linear attention, adding DWC to image features consistently improves performance (i.e., FID and IS) across model sizes. We attribute this to the limited locality of linear attention used, which remains a bottleneck in autoregressive image generation. Introducing an appropriate inductive bias, e.g., depthwise convolution, appears beneficial for parameter scaling. Developing effective ways to enhance locality remains an interesting direction for future work. From now on, we will use division-based linear attention with DWC as our basic design choice.

## 5. KV Gate For Flexible Memory Management

Gating mechanism (Yang et al., 2024; 2025; Sun et al., 2023; 2024b; Dao & Gu, 2024; Schlag et al., 2021), a common practice in autoregressive language models, help flexibly manage memory. In *causal* linear attention, they are typically implemented as data-dependent decay terms to selectively “forget” past information. Gating factor not only preserves efficiency but also shows potential in language modeling, *etc.* (Yang et al., 2025). However, their use in

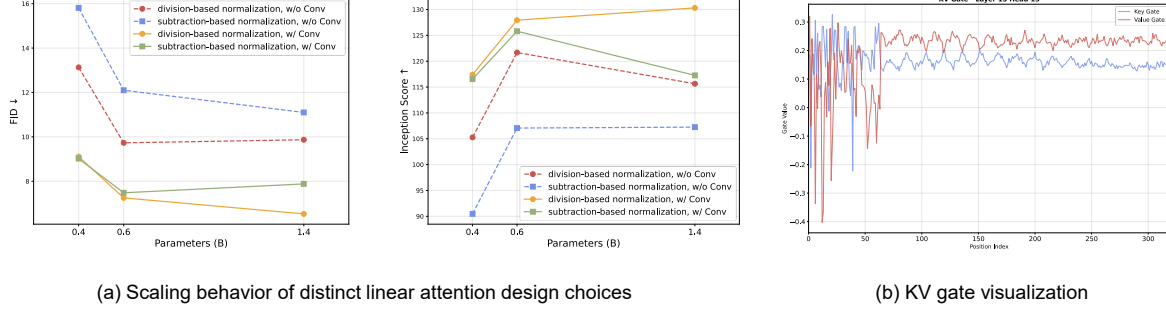


**Figure 4. Scaling behavior and KV gate results.** Fig. (a) describes the class-conditional image generation results on the ImageNet 256×256 benchmark using FID (↓) and IS (↑). Division-based linear attention with LAM achieves the best scaling performance. Detailed results are provided in Appendix G. Fig. (b) presents the learned KV gate of a 256px text-to-image LINA model.

settings that require *bidirectional* attention (e.g., autoregressive image models) remains underexplored. We believe the key lies in the difference between causal and bidirectional mechanisms. Denote the memory as  $M$ . In causal attention, the forget gate  $\alpha$  is used to “erase” past information, *i.e.*,  $M_t = \alpha_t M_{t-1} + K_t^\top V_t$  (assume  $\phi(\cdot)$  is identity function). However, in bidirectional attention, there is no causal mask and thus no notion of a strict “past”: tokens at any positions in the sequence can attend to each other. Therefore, we argue that the memories  $M_i$  and  $M_j$  at arbitrary positions  $i$  and  $j$  should not have a forget–retain relationship. Instead, they should be assigned different importance weights.

To this end, we propose a simple yet effective method, called *KV gate*, to equip bidirectional linear attention with gating. We express linear attention (Eq. 2) as the following form:

$$M = \sum_{j=1}^N \phi(K_j)^\top V_j, z = \sum_{m=1}^N \phi(K_m)^\top, O_i^{(a)} = \frac{\phi(Q_i)M}{\phi(Q_i)z}, \quad (6)$$

where memory  $M \in \mathbb{R}^{D \times D}$  represents the *equally weighted sum* of token-wise memories  $M_i$ , while  $z \in \mathbb{R}^{D \times 1}$  contributes to the normalization term  $\gamma_i^{(a)} = \phi(Q_i)z$ .

In a nutshell, we use a learnable *K gate* to scale both  $M$  and  $z$ , and another learnable *V gate* to scale  $M$  only. This method, dubbed *KV gate*, allows effective and flexible memory arrangement. Division-based normalization linear attention (Eq. 6) using the *KV gate* can be formulated as follows:

$$\begin{aligned} \tilde{K}_j &= g_j^{(k)} \phi(K_j), \quad \tilde{V}_j = g_j^{(v)} V_j, \quad \text{for } j \in [1, N] \\ M &= \sum_{j=1}^N \tilde{K}_j^\top \tilde{V}_j = \sum_{j=1}^N g_j^{(k)} g_j^{(v)} M_j, \\ z &= \sum_{m=1}^N \tilde{K}_m^\top, \quad O_i^{(a)} = \frac{\phi(Q_i)M}{\phi(Q_i)z}, \end{aligned} \quad (7)$$

where the *K gate*  $g^{(k)}$  denotes the scaling coefficient applied to  $\phi(K)$  when computing both  $M$  and  $z$ , while the *V gate*

**Table 1. Ablation study of KV gate.** ImageNet 256×256 results (w/o CFG) are reported. All models are trained for 200K iterations. Head-wise KV gate are chosen. HW: head-wise. HS: head-shared.

Gate	Key	Value	$z^{(a)}$	FID ↓	sFID ↓	IS ↑	Pre. ↑	Rec. ↑
None				9.11	5.89	117.40	0.69	0.61
HW	✓	✓		<b>8.72</b>	5.64	<b>120.34</b>	0.69	0.61
HW	✓			8.80	5.69	119.20	0.70	0.62
HW		✓		9.06	5.60	115.90	0.69	0.61
HW	✓	✓	✓	9.22	5.89	115.41	0.69	0.61
HS	✓	✓		<b>8.72</b>	5.70	120.24	0.69	0.62

$g^{(v)}$  serves as an auxiliary part that adjusts  $M$  only.

KV gate is applied in all linear attention in the *Decoder* of our model. Besides the KV gate, we also design three variants as ablations, *i.e.*, *K gate only*, *V gate only*, and a variant with an *extra gate* applied to  $z$  (see Appendix E for details of the four modes). Ablation study is conducted on ImageNet class-conditional image generation task using a  $\sim 0.4$ B model.

As reported in Tab. 1, KV gate consistently improves FID, IS, and sFID compared to division-based normalization linear attention baseline. We present two thought-provoking findings. (1) Using only V gate or applying an extra gate to  $z$  severely degrades FID and IS. (2) Using only K gate slightly affects FID and IS. This indicates that the K gate and V gate exhibit a synergistic effect rather than being mutually exclusive. Moreover, we suggest leveraging the K gate to scale  $z$ , instead of introducing an additional set of learnable coefficients. With  $h$  attention heads, the KV gate introduces only  $2 \times h \times N \times L_D \approx 0.12$ M parameters for a sequence length of  $N = 320$ , which is negligible compared to the  $\sim 0.4$ B parameters of the model.

**Should the KV gate be head-wise or head-shared?** We investigate whether the KV gates across different attention heads should share parameters. As shown in Tab. 1, using a head-specific KV gate slightly improves IS and sFID. Given its negligible parameter overhead, we adopt the head-wise design. We kindly note that (Lin et al., 2025; Qiu et al., 2025) investigate incorporating gating mechanisms

into softmax attention.

**What pattern has the KV gate learned?** As shown in Fig. 4-(b), we visualize the KV gate of LINA-H trained for 500K iterations at 256px resolution on text-to-image generation task to illustrate specific patterns they have learned. For the first 64 query tokens, the values of the KV gate exhibit fluctuations, while for the subsequent 256 image tokens, they are more stable and display a clear periodic pattern. Notably, K gate peak when V gate dip, indicating complementary roles in memory management in the linear attention. Additional results (provided in Appendix I) show that, although we do not explicitly restrict the KV gate values, they generally remain within the interval  $(0, 1)$  and display diverse patterns across different layers and heads. See Appendix I for detailed results.

**Difference between KV gate and the forget gate.** Forget gate in GLA and our KV gate both modulates memory but differs in three ways. **(1) Recurrence vs. parallelism:** Forget gate is recursive—its decay factor for  $M_j$  is  $\prod_{s=j+1}^t \alpha_s$ . In contrast, our KV gate computes the factor  $g_j^{(k)} g_j^{(v)}$  once without recurrence. **(2) Data dependence:** Forget gate is typically data-dependent, with  $\alpha_t$  projected from the current input token (Yang et al., 2024). Differently, KV gate is data-independent. We find that simple learnable parameters is sufficient to improve performance without linear projection. **(3) Range constraint:** Forget gate (Sun et al., 2024b) restricts  $\alpha_t$  to  $(0, 1)$  due to the sigmoid function, whereas KV gate allows  $g_j^{(k)}, g_j^{(v)}$  to be negative, supporting flexible learning.

## 6. Experiments

### 6.1. Class-conditional Image Generation

**Training details.** As an system-level validation of our method, we conduct class-conditional image generation experiments on the ImageNet 256×256 benchmark using LINA-H (1.4B). Using a learning rate of  $8 \times 10^{-4}$  and a batch size of 768, we train the model for a total of 1.2M iterations. We set the model EMA (Polyak & Juditsky, 1992) to 0.99 and the weight decay to 0.02. Following NOVA, we adopt a 6-layer flow matching MLP as the denoising network, without relying on advanced training approaches, *e.g.*, REPA (Yu et al., 2024b). Sampling during inference is done in BFfloat16 precision. The autoregressive and diffusion steps are set at 64 and 25, respectively. We report results with CFG scale of 1.0 and 2.4.

**Results.** In Tab. 2, we present a system-level evaluation of LINA against other frontier models. Compared with the linear diffusion model (*e.g.*, LiT (Wang et al., 2025)) and the full attention autoregressive model (*e.g.*, MAR), LINA—based on a linear autoregressive architecture—delivers

Table 2. Class-conditional ImageNet 256×256 results.

Model	FID ↓	IS ↑	Precision ↑	Recall ↑
<i>Diffusion models</i>				
ADM (Dhariwal & Nichol, 2021)	4.59	186.70	0.82	0.52
CDM (Ho et al., 2022)	4.88	158.71	-	-
LDM-4 (Rombach et al., 2022)	3.60	247.67	0.87	0.48
U-ViT-H/2-G (Bao et al., 2022)	2.29	263.9	0.82	0.57
DiT-XL/2 (Peebles & Xie, 2023)	2.27	278.24	0.83	0.57
LiT-XL/2 (Wang et al., 2025)	2.32	265.20	0.824	0.574
DiffuSSM-XL-G (Yan et al., 2024)	2.28	259.13	0.86	0.56
DiM-L (Teng et al., 2024)	2.64	-	-	-
DiM-H (Teng et al., 2024)	2.21	-	-	-
DiG-XL/2-G (Zhu et al., 2024)	2.07	278.95	0.82	0.60
SiT-XL (Ma et al., 2024)	2.06	277.50	0.83	0.59
Mediator (Pu et al., 2024)	2.01	271.04	0.82	0.60
<i>Autoregressive models</i>				
Mask-GIT (Chang et al., 2022)	6.18	182.1	-	-
MAGVIT-v2 (Yu et al., 2024a)	<b>1.78</b>	<b>319.4</b>	-	-
MAR-B (Li et al., 2024b)	2.31	281.7	0.82	0.57
MAR-L	<b>1.78</b>	<b>296.0</b>	0.81	0.60
LINA-H (cfg=1.0)	4.49	162.64	0.74	0.62
LINA-H (cfg=2.4)	2.18	275.73	0.81	0.58

competitive performance. Notably, LINA-H achieves an FID of 2.18, demonstrating that the linear attention designed in this work is well suited for autoregressive image modeling. In addition, LINA attains superior validated performance than DiM, an efficient state space model (Gu & Dao, 2023; Dao & Gu, 2024) based diffusion model. As a result, we turn to validate LINA on text-to-image benchmarks.

### 6.2. Text-to-image Generation

**Training details.** Our training pipeline consists of three stages. Following LiT, we initialize stage 1 with the 1024px NOVA pretrained weights, excluding the linear attention. The three stages are trained on 256px, 512px, and 1024px data, respectively. Training is conducted on 48 A100 (40GB) GPUs with batch sizes of 768, 192, and 48. Stages 2 and 3 run for 600K and 700K iterations. We set 128 autoregressive steps and 25 diffusion steps, with a CFG scale of 7.0 during sampling. Details are provided in Appendix H.

**Results.** As shown in Tab. 3, we compare LINA with advanced text-to-image architectures on the GenEval benchmark (Ghosh et al., 2023). Without prompt engineering, the 1.4B LINA outperforms the 1.6B SANA, an advanced linear DiT baseline. Moreover, compared with autoregressive models using full attention, LINA achieves performance on par with the 10.5B Fluid. These results demonstrate that the proposed linear attention integrates well with autoregressive architectures and exhibits strong text-image alignment, providing a clear and reliable baseline. Fig. 1 shows 1024px samples generated by LINA, where image fidelity and fine textures are well-preserved across long sequences.

**FLOPs comparison: softmax attention vs. linear attention in LINA.** We report the FLOPs of a single attention module under the following configuration: batch size of 1, sequence length of 5120, hidden dimension of 1536, and 16

Table 3. Comparison of GenEval results. Rewriter refers to a prompt engineering method (Deng et al., 2025). Our LINA, equipped with pure linear attention, rivals advanced T2I frameworks. Best results are in **bold**; second best are underlined.

Model	Params.	Overall	Single	Two	Counting	Colors	Position	ColorAttr
<i>Diffusion models</i>								
PixArt- $\alpha$ (Chen et al., 2024b)	0.6B	0.48	0.98	0.50	0.44	0.80	0.08	0.07
LiT (1024×1024) (Wang et al., 2025)	0.6B	0.48	0.98	0.50	0.40	0.77	0.11	0.12
LiT (512×512)	0.6B	0.47	0.97	0.43	0.42	0.79	0.09	0.12
DALL-E3 (OpenAI, 2023)	-	0.67	0.96	0.87	0.47	0.83	0.43	0.45
SDXL (Podell et al., 2023)	2.6B	0.55	0.98	0.44	0.39	0.85	0.15	0.23
SD3 (Esser et al., 2024)	2B	0.62	0.98	0.74	0.63	0.67	0.34	0.36
Playground v2.5 (Li et al., 2024a)	2.6B	<u>0.56</u>	-	-	-	-	-	-
Hunyuan-DiT (Li et al., 2024c)	1.5B	0.63	-	-	-	-	-	-
SANA (1024×1024) (Xie et al., 2025a)	1.6B	0.66	-	-	-	-	-	-
SANA (512×512)	1.6B	0.66	-	-	-	-	-	-
<i>Autoregressive models</i>								
LlamaGen (Sun et al., 2024a)	0.8B	0.32	0.71	0.34	0.21	0.58	0.07	0.04
Emu3 (+ Rewriter) (Wang et al., 2024)	8B	0.66	0.99	0.81	0.42	0.80	0.49	0.45
Show-o (Xie et al., 2024)	1.3B	0.53	0.95	0.52	0.49	0.82	0.11	0.28
NOVA (1024×1024) (Deng et al., 2025)	1.4B	0.71	0.99	0.91	0.62	0.85	0.33	0.56
NOVA (512×512) (+ Rewriter)	0.6B	<b>0.75</b>	0.98	0.88	0.62	0.82	0.62	0.58
Fluid (Fan et al., 2025a)	1.1B	0.67	0.96	0.77	0.61	0.78	0.34	0.53
Fluid (Fan et al., 2025a)	10.5B	0.69	0.96	0.83	0.63	0.80	0.39	0.51
LINA-H (1024×1024)	1.5B	0.66	0.99	0.85	0.50	0.88	0.38	0.39
+ Rewriter	1.5B	0.72	0.99	0.84	0.54	0.85	0.56	0.53
LINA-H (512×512)	1.4B	0.68	0.98	0.83	0.56	0.89	0.34	0.50
+ Rewriter	1.4B	<u>0.74</u>	0.99	0.85	0.61	0.87	0.60	0.53

attention heads. This setup matches how LINA-H operates at a resolution of 1024px. The linear attention module we evaluate adopts *division-based normalization* in the LINA *Decoder* and integrates both the *DWC module* and the *KV gate* proposed in this work. FLOPs are measured using the fvcore (fvcore Contributors, 2021) library.

The results are presented in Fig. 5. Softmax attention requires approximately  $\sim$ 129 GFLOPs, whereas the linear attention requires only  $\sim$ 50 GFLOPs. This corresponds to a reduction of about  $\sim$ 61% in FLOPs, highlighting the efficiency of our LINA. Importantly, despite this substantial reduction in FLOPs, the T2I performance of LINA remains competitive with softmax attention-based NOVA. Note that *DWC module* and *KV gate* are used only in the LINA *Decoder*, and are not applied in the *Encoder* or the *Connector*.

**Latency comparison.** Tab. 4 reports the pipeline latency comparison between NOVA and LINA when generating 1024px images. LINA shares the same macro architecture as NOVA, but completely replaces NOVA’s softmax attention with linear attention. For each run, we compute the average latency of generating 10 images, and the reported latency is the mean over three such runs. All experiments are conducted on a NVIDIA A800 GPU with a batch size of 1. Since our work represents an early exploration of linear MAR models with an emphasis on sample quality, we do not incorporate additional acceleration techniques, *e.g.*, Triton (Tillet et al., 2019). Even without such optimizations, LINA attains latency on par with softmax attention using FlashAttention (Dao et al., 2022). We attribute this parity to

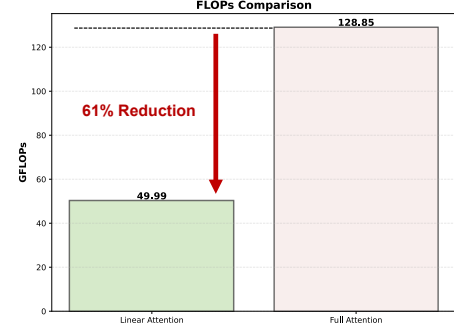


Figure 5. FLOPs comparison: **a single module of linear attention vs. softmax attention**. We use a batch size of 1, a sequence length of 5120, a hidden dimension of 1536, and 16 attention heads. Such configuration corresponds to how LINA-H operates at 1024px. Linear attention applies division-based normalization and incorporates both the *DWC module* and the *KV gate*. Compared with softmax attention, linear attention reduces FLOPs by  $\sim$ 61%, showing computation efficiency.

the inherent computational advantage of linear attention in processing long sequences.

Table 4. Latency comparison results. LINA competes FlashAttention in 1024px generation.

Model	Params.	Res.	Type	Acceleration	Latency
NOVA	1.4B	1024px	Softmax	FlashAttn	20.0s
LINA	1.5B	1024px	Linear	-	22.0s

## 7. Conclusion

This paper takes a deep dive into how linear attention should be designed for autoregressive image generative model with continuous tokens. We recommend adopting division-based normalization and incorporating convolution to strengthen locality. Besides, we introduce the KV gate, a simple way that modulates key and value states to enable flexible memory management and, in turn, improve generation. Our final model, dubbed LINA, is an linear autoregressive model that delivers competitive image generation performance.

## Impact Statements

This paper presents work whose goal is to advance the field of machine learning, with a focus on efficient autoregressive image generation. There are many potential societal consequences of generative models, none of which we feel must be specifically highlighted here beyond those already well studied in the literature.

## References

Bao, F., Li, C., Cao, Y., and Zhu, J. All are worth words: a vit backbone for score-based diffusion models. In *NeurIPS Workshop*, 2022.

Cai, H., Li, J., Hu, M., Gan, C., and Han, S. Efficientvit: Multi-scale linear attention for high-resolution dense prediction. In *ICCV*, 2023.

Chang, H., Zhang, H., Jiang, L., Liu, C., and Freeman, W. T. Maskgit: Masked generative image transformer. In *CVPR*, 2022.

Chen, J., Ge, C., Xie, E., Wu, Y., Yao, L., Ren, X., Wang, Z., Luo, P., Lu, H., and Li, Z. Pixart- $\sigma$ : Weak-to-strong training of diffusion transformer for 4k text-to-image generation. In *ECCV*, 2024a.

Chen, J., Yu, J., Ge, C., Yao, L., Xie, E., Wu, Y., Wang, Z., Kwok, J., Luo, P., Lu, H., et al. Pixart- $\alpha$ : Fast training of diffusion transformer for photorealistic text-to-image synthesis. In *ICLR*, 2024b.

Chen, J., Xue, S., Zhao, Y., Yu, J., Paul, S., Chen, J., Cai, H., Han, S., and Xie, E. Sana-sprint: One-step diffusion with continuous-time consistency distillation. In *ICCV*, 2025.

Chollet, F. Xception: Deep learning with depthwise separable convolutions. In *CVPR*, 2017.

Choromanski, K., Likhoshesterov, V., Dohan, D., Song, X., Gane, A., Sarlos, T., Hawkins, P., Davis, J., Mohiuddin, A., Kaiser, L., et al. Rethinking attention with performers. In *ICLR*, 2021.

Cordonnier, J.-B., Loukas, A., and Jaggi, M. On the relationship between self-attention and convolutional layers. *arXiv preprint arXiv:1911.03584*, 2019.

Dao, T. and Gu, A. Transformers are ssms: Generalized models and efficient algorithms through structured state space duality. In *ICML*, 2024.

Dao, T., Fu, D., Ermon, S., Rudra, A., and Ré, C. Flashattention: Fast and memory-efficient exact attention with io-awareness. In *NeurIPS*, 2022.

Dehghani, M., Djolonga, J., Mustafa, B., Padlewski, P., Heek, J., Gilmer, J., Steiner, A. P., Caron, M., Geirhos, R., Alabdulmohsin, I., et al. Scaling vision transformers to 22 billion parameters. In *ICML*, 2023.

Deng, H., Pan, T., Diao, H., Luo, Z., Cui, Y., Lu, H., Shan, S., Qi, Y., and Wang, X. Autoregressive video generation without vector quantization. In *ICLR*, 2025.

Deng, J., Dong, W., Socher, R., Li, L.-J., Li, K., and Fei-Fei, L. Imagenet: A large-scale hierarchical image database. In *CVPR*, 2009.

Dhariwal, P. and Nichol, A. Diffusion models beat gans on image synthesis. In *NeurIPS*, 2021.

Dosovitskiy, A., Beyer, L., Kolesnikov, A., Weissenborn, D., Zhai, X., Unterthiner, T., Dehghani, M., Minderer, M., Heigold, G., Gelly, S., et al. An image is worth 16x16 words: Transformers for image recognition at scale. In *ICLR*, 2020.

Esser, P., Kulal, S., Blattmann, A., Entezari, R., Müller, J., Saini, H., Levi, Y., Lorenz, D., Sauer, A., Boesel, F., et al. Scaling rectified flow transformers for high-resolution image synthesis. In *ICML*, 2024.

Fan, L., Li, T., Qin, S., Li, Y., Sun, C., Rubinstein, M., Sun, D., He, K., and Tian, Y. Fluid: Scaling autoregressive text-to-image generative models with continuous tokens. In *ICLR*, 2025a.

Fan, Q., Huang, H., Ai, Y., and He, R. Rectifying magnitude neglect in linear attention. In *ICCV*, 2025b.

fvcore Contributors. fvcore. <https://github.com/facebookresearch/fvcore>, 2021.

Ghosh, D., Hajishirzi, H., and Schmidt, L. Geneval: An object-focused framework for evaluating text-to-image alignment. In *NeurIPS*, 2023.

Gu, A. and Dao, T. Mamba: Linear-time sequence modeling with selective state spaces. *arXiv preprint arXiv:2312.00752*, 2023.

Guo, J., Chen, X., Tang, Y., and Wang, Y. Slab: Efficient transformers with simplified linear attention and progressive re-parameterized batch normalization. In *ICML*, 2024.

Han, D., Pan, X., Han, Y., Song, S., and Huang, G. Flatten transformer: Vision transformer using focused linear attention. In *ICCV*, 2023.

Han, D., Pu, Y., Xia, Z., Han, Y., Pan, X., Li, X., Lu, J., Song, S., and Huang, G. Bridging the divide: Reconsidering softmax and linear attention. In *NeurIPS*, 2024.

Heusel, M., Ramsauer, H., Unterthiner, T., Nessler, B., and Hochreiter, S. Gans trained by a two time-scale update rule converge to a local nash equilibrium. In *NeurIPS*, 2017.

Ho, J. and Salimans, T. Classifier-free diffusion guidance. *arXiv preprint arXiv:2207.12598*, 2022.

Ho, J., Jain, A., and Abbeel, P. Denoising diffusion probabilistic models. In *NeurIPS*, 2020.

Ho, J., Saharia, C., Chan, W., Fleet, D. J., Norouzi, M., and Salimans, T. Cascaded diffusion models for high fidelity image generation. *Journal of Machine Learning Research*, 2022.

Howard, A. G., Zhu, M., Chen, B., Kalenichenko, D., Wang, W., Weyand, T., Andreetto, M., and Adam, H. Mobilenets: Efficient convolutional neural networks for mobile vision applications. In *CVPR*, 2017.

Hui, M., Zhu, R.-J., Yang, S., Zhang, Y., Wang, Z., Zhou, Y., Eshraghian, J., and Xie, C. Arflow: Autoregressive flow with hybrid linear attention. *arXiv preprint arXiv:2501.16085*, 2025.

Katharopoulos, A., Vyas, A., Pappas, N., and Fleuret, F. Transformers are rnns: Fast autoregressive transformers with linear attention. In *ICML*, 2020.

Kynkänniemi, T., Karras, T., Laine, S., Lehtinen, J., and Aila, T. Improved precision and recall metric for assessing generative models. In *NeurIPS*, 2019.

Li, D., Kamko, A., Akhgari, E., Sabet, A., Xu, L., and Doshi, S. Playground v2. 5: Three insights towards enhancing aesthetic quality in text-to-image generation. *arXiv preprint arXiv:2402.17245*, 2024a.

Li, T., Tian, Y., Li, H., Deng, M., and He, K. Autoregressive image generation without vector quantization. In *NeurIPS*, 2024b.

Li, Z., Zhang, J., Lin, Q., Xiong, J., Long, Y., Deng, X., Zhang, Y., Liu, X., Huang, M., Xiao, Z., et al. Hunyuan-dit: A powerful multi-resolution diffusion transformer with fine-grained chinese understanding. *arXiv preprint arXiv:2405.08748*, 2024c.

Lin, Z., Nikishin, E., He, X. O., and Courville, A. Forgetting transformer: Softmax attention with a forget gate. *arXiv preprint arXiv:2503.02130*, 2025.

Lipman, Y., Chen, R. T., Ben-Hamu, H., Nickel, M., and Le, M. Flow matching for generative modeling. In *ICLR*, 2023.

Liu, X., Gong, C., and Liu, Q. Flow straight and fast: Learning to generate and transfer data with rectified flow. In *ICLR*, 2023.

Liu, Z., Mao, H., Wu, C.-Y., Feichtenhofer, C., Darrell, T., and Xie, S. A convnet for the 2020s. In *CVPR*, 2022.

Lu, C. and Song, Y. Simplifying, stabilizing and scaling continuous-time consistency models. *arXiv preprint arXiv:2410.11081*, 2024.

Ma, N., Goldstein, M., Albergo, M. S., Boffi, N. M., Vandeneijnden, E., and Xie, S. Sit: Exploring flow and diffusion-based generative models with scalable interpolant transformers. In *ECCV*, 2024.

Nash, C., Menick, J., Dieleman, S., and Battaglia, P. W. Generating images with sparse representations. *arXiv preprint arXiv:2103.03841*, 2021.

OpenAI. Dalle-3, 2023. URL <https://openai.com/dalle-3>.

Peebles, W. and Xie, S. Scalable diffusion models with transformers. In *ICCV*, 2023.

Podell, D., English, Z., Lacey, K., Blattmann, A., Dockhorn, T., Müller, J., Penna, J., and Rombach, R. Sdxl: Improving latent diffusion models for high-resolution image synthesis. *arXiv preprint arXiv:2307.01952*, 2023.

Polyak, B. T. and Juditsky, A. B. Acceleration of stochastic approximation by averaging. *SIAM journal on control and optimization*, 1992.

Pu, Y., Xia, Z., Guo, J., Han, D., Li, Q., Li, D., Yuan, Y., Li, J., Han, Y., Song, S., et al. Efficient diffusion transformer with step-wise dynamic attention mediators. In *ECCV*, 2024.

Pu, Y., Ying, J., Li, Q., Ye, T., Han, D., Wang, X., Wang, Z., Shao, X., Huang, G., and Li, X. Linear differential vision transformer: Learning visual contrasts via pairwise differentials. *arXiv preprint arXiv:2511.00833*, 2025.

Qiu, Z., Wang, Z., Zheng, B., Huang, Z., Wen, K., Yang, S., Men, R., Yu, L., Huang, F., Huang, S., et al. Gated attention for large language models: Non-linearity, sparsity,

and attention-sink-free. *arXiv preprint arXiv:2505.06708*, 2025.

Rombach, R., Blattmann, A., Lorenz, D., Esser, P., and Ommer, B. High-resolution image synthesis with latent diffusion models. In *CVPR*, 2022.

Salimans, T., Goodfellow, I., Zaremba, W., Cheung, V., Radford, A., and Chen, X. Improved techniques for training gans. In *NeurIPS*, 2016.

Schlag, I., Irie, K., and Schmidhuber, J. Linear transformers are secretly fast weight programmers. In *ICML*, 2021.

Sohl-Dickstein, J., Weiss, E., Maheswaranathan, N., and Ganguli, S. Deep unsupervised learning using nonequilibrium thermodynamics. In *ICML*, 2015.

Song, Y., Dhariwal, P., Chen, M., and Sutskever, I. Consistency models. 2023.

Sun, P., Jiang, Y., Chen, S., Zhang, S., Peng, B., Luo, P., and Yuan, Z. Autoregressive model beats diffusion: Llama for scalable image generation. *arXiv preprint arXiv:2406.06525*, 2024a.

Sun, Y., Dong, L., Huang, S., Ma, S., Xia, Y., Xue, J., Wang, J., and Wei, F. Retentive network: A successor to transformer for large language models. *arXiv preprint arXiv:2307.08621*, 2023.

Sun, Y., Dong, L., Zhu, Y., Huang, S., Wang, W., Ma, S., Zhang, Q., Wang, J., and Wei, F. You only cache once: Decoder-decoder architectures for language models. In *NeurIPS*, 2024b.

Team, N., Han, C., Li, G., Wu, J., Sun, Q., Cai, Y., Peng, Y., Ge, Z., Zhou, D., Tang, H., et al. Nextstep-1: Toward autoregressive image generation with continuous tokens at scale. *arXiv preprint arXiv:2508.10711*, 2025.

Teng, Y., Wu, Y., Shi, H., Ning, X., Dai, G., Wang, Y., Li, Z., and Liu, X. Dim: Diffusion mamba for efficient high-resolution image synthesis. *arXiv preprint arXiv:2405.14224*, 2024.

Tillet, P., Kung, H.-T., and Cox, D. Triton: an intermediate language and compiler for tiled neural network computations. In *Proceedings of the 3rd ACM SIGPLAN International Workshop on Machine Learning and Programming Languages*, 2019.

Touvron, H., Cord, M., Douze, M., Massa, F., Sablayrolles, A., and Jégou, H. Training data-efficient image transformers & distillation through attention. In *ICML*, 2021.

Vaswani, A., Shazeer, N., Parmar, N., Uszkoreit, J., Jones, L., Gomez, A. N., Kaiser, L., and Polosukhin, I. Attention is all you need. In *NIPS*, 2017.

Wang, J., Kang, N., Yao, L., Chen, M., Wu, C., Zhang, S., Xue, S., Liu, Y., Wu, T., Liu, X., et al. Lit: Delving into a simplified linear diffusion transformer for image generation. In *ICCV*, 2025.

Wang, X., Zhang, X., Luo, Z., Sun, Q., Cui, Y., Wang, J., Zhang, F., Wang, Y., Li, Z., Yu, Q., et al. Emu3: Next-token prediction is all you need. *arXiv preprint arXiv:2409.18869*, 2024.

Woo, S., Debnath, S., Hu, R., Chen, X., Liu, Z., Kweon, I. S., and Xie, S. Convnext v2: Co-designing and scaling convnets with masked autoencoders. In *CVPR*, 2023.

Wu, Y., Chen, J., Zhang, Z., Xie, E., Yu, J., Chen, J., Hu, J., Lu, Y., Han, S., and Cai, H. Dc-ar: Efficient masked autoregressive image generation with deep compression hybrid tokenizer. In *ICCV*, 2025.

Xie, E., Chen, J., Chen, J., Cai, H., Lin, Y., Zhang, Z., Li, M., Lu, Y., and Han, S. Sana: Efficient high-resolution image synthesis with linear diffusion transformers. In *ICLR*, 2025a.

Xie, E., Chen, J., Zhao, Y., Yu, J., Zhu, L., Wu, C., Lin, Y., Zhang, Z., Li, M., Chen, J., et al. Sana 1.5: Efficient scaling of training-time and inference-time compute in linear diffusion transformer. In *ICML*, 2025b.

Xie, J., Mao, W., Bai, Z., Zhang, D. J., Wang, W., Lin, K. Q., Gu, Y., Chen, Z., Yang, Z., and Shou, M. Z. Show-o: One single transformer to unify multimodal understanding and generation. *arXiv preprint arXiv:2408.12528*, 2024.

Yan, F., Wei, Q., Tang, J., Li, J., Wang, Y., Hu, X., Li, H., and Zhang, L. Lazymar: Accelerating masked autoregressive models via feature caching. In *ICCV*, 2025.

Yan, J. N., Gu, J., and Rush, A. M. Diffusion models without attention. In *CVPR*, 2024.

Yang, S., Wang, B., Shen, Y., Panda, R., and Kim, Y. Gated linear attention transformers with hardware-efficient training. In *ICML*, 2024.

Yang, S., Kautz, J., and Hatamizadeh, A. Gated delta networks: Improving mamba2 with delta rule. In *ICLR*, 2025.

Yin, T., Gharbi, M., Park, T., Zhang, R., Shechtman, E., Durand, F., and Freeman, W. T. Improved distribution matching distillation for fast image synthesis. In *NeurIPS*, 2024a.

Yin, T., Gharbi, M., Zhang, R., Shechtman, E., Durand, F., Freeman, W. T., and Park, T. One-step diffusion with distribution matching distillation. In *CVPR*, 2024b.

Yin, T., Zhang, Q., Zhang, R., Freeman, W. T., Durand, F., Shechtman, E., and Huang, X. From slow bidirectional to fast autoregressive video diffusion models. In *CVPR*, 2025.

Yu, L., Lezama, J., Gundavarapu, N. B., Versari, L., Sohn, K., Minnen, D., Cheng, Y., Birodkar, V., Gupta, A., Gu, X., et al. Language model beats diffusion–tokenizer is key to visual generation. In *ICLR*, 2024a.

Yu, S., Kwak, S., Jang, H., Jeong, J., Huang, J., Shin, J., and Xie, S. Representation alignment for generation: Training diffusion transformers is easier than you think. *arXiv preprint arXiv:2410.06940*, 2024b.

Zhang, Y., Yang, S., Zhu, R.-J., Zhang, Y., Cui, L., Wang, Y., Wang, B., Shi, F., Wang, B., Bi, W., et al. Gated slot attention for efficient linear-time sequence modeling. In *NeurIPS*, 2024.

Zhao, Q., Singh, J., Xu, M., Asthana, A., Gould, S., and Zheng, L. Disa: Diffusion step annealing in autoregressive image generation. *arXiv preprint arXiv:2505.20297*, 2025.

Zhu, L., Huang, Z., Liao, B., Liew, J. H., Yan, H., Feng, J., and Wang, X. Dig: Scalable and efficient diffusion models with gated linear attention. *arXiv preprint arXiv:2405.18428*, 2024.

## A. Full Related Work

Efficiency is a key concern for image generative models when dealing with long sequences. Research on efficient diffusion models is relatively extensive. Some approaches focus on architectural modifications, especially efficient attention (Katharopoulos et al., 2020; Choromanski et al., 2021; Yang et al., 2024; Cai et al., 2023; Han et al., 2023). For example, SANA (Xie et al., 2025a) studies the text encoder in text-to-image models, while LiT (Wang et al., 2025) provides guidelines for converting a pretrained DiT into a linear DiT. DiG (Zhu et al., 2024) and DiM (Teng et al., 2024) explore applying gated linear attention and state space models (Gu & Dao, 2023; Dao & Gu, 2024), respectively, to image generation. Other works pursue fewer or even single diffusion steps, such as DMD (Yin et al., 2024b), DMD2 (Yin et al., 2024a), CausVid (Yin et al., 2025), consistency models (Song et al., 2023; Lu & Song, 2024), and SANA-Sprint (Chen et al., 2025).

For autoregressive models with continuous tokens, researchers have explored various directions to improve efficiency. Notably, DiSA (Zhao et al., 2025) reduces the number of diffusion steps as the autoregressive process progresses. Lazy-MAR (Yan et al., 2025) explores how to use feature caching to improve efficiency while maintaining performance. DC-AR (Wu et al., 2025) studies the design and training of image tokenizer. ARFlow (Hui et al., 2025) enables flow-based image generation through hybrid linear attention.

## B. Inference Pipeline

As described in Fig. 6-(a), LINA inference pipeline starts by encoding the text prompt with a text encoder and integrating it into the query token through the Connector. The image generation process starts with all tokens masked and proceeds through a multi-step, generalized autoregressive procedure that generates image tokens progressively. At each step, the Encoder extracts information from the predicted tokens, which—together with the masked tokens—are decoded by the Decoder to form the conditioning. A denoising flow matching network (e.g., MLP) samples the token based on this conditioning. After all autoregressive steps, the generated tokens are feed into a VAE decoder to produce the final image.

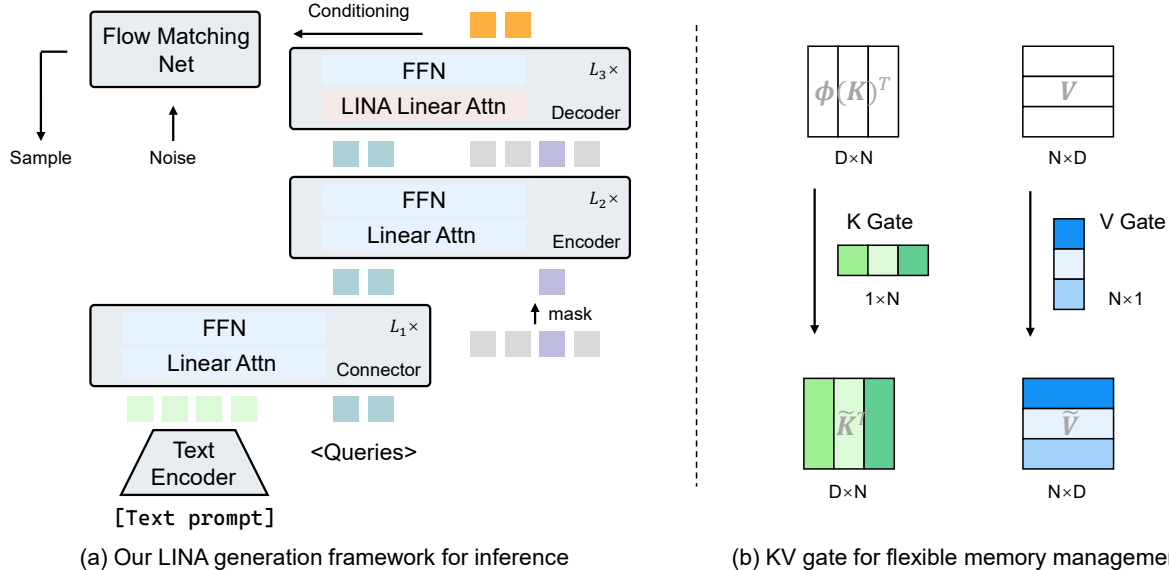


**Figure 6. Overview of LINA:** Fig. (a) illustrates the inference pipeline. LINA builds its Connector, Encoder, and Decoder entirely with linear attention in pursuit of efficiency. At each step, the Encoder and Decoder predict the conditioning from the known tokens, after which the denoising network draws sample based on the conditioning.

## C. Model Configuration

The detailed configurations of our LINA models of varying sizes for class-conditional image generation are listed in Tab. 5, corresponding to the exploration roadmap discussed in Sec. 4. Tab. 6 reports the detailed hyperparameters of LINA for both class-conditional and text-to-image generation in our main experiments in Sec. 6.

## D. Detailed hyper-parameters on ImageNet-1K in Sec. 4

In Tab. 7, we provide the hyper-parameters for the experiments in Sec. 4, which explore the scaling behavior of different linear attention design choices.

Table 5. Detailed LINA configurations in Sec. 4.

Configuration	L	XL	H
Task	C2I	C2I	C2I
Resolution	256px	256px	256px
Params (M)	0.4B	0.6B	1.4B
Connector Blocks	16	16	16
Encoder Blocks	16	16	16
Decoder Blocks	16	16	16
Flow Matching MLP Depth	6	6	6
Channels	768	1024	1536
DWC Kernel Size	5	5	5

Table 6. Detailed LINA configurations in Sec. 6.

Configuration	H	H	H
Task	C2I	T2I	T2I
Resolution	256px	512px	1024px
Params (M)	1.4B	1.4B	1.5B
Connector Blocks	16	16	16
Encoder Blocks	16	16	16
Decoder Blocks	16	16	16
Flow Matching MLP Depth	6	6	6
Channels	1536	1536	1536
DWC Kernel Size	5	5	5

Table 7. Training setting of LINA for scaling behavior empirical study in Sec. 4.

Training Setting	L	XL	H
Base Learning Rate	$8 \times 10^{-4}$	$8 \times 10^{-4}$	$8 \times 10^{-4}$
Batch Size	64×32	48×32	24×32
Training Iteration	200K	200K	200K
Weight Decay	0.02	0.02	0.02
Warm-up Steps	10000	10000	10000
Model EMA	0.99	0.99	0.99

## E. Complexity analysis of DWC Module and KV Gate

Following VCA (Pu et al., 2025), we provide a complexity analysis to the DWC module and KV gate used in LINA. We follow the notation in Sec. 3: assume the model uses  $H$  attention heads to process  $N = N_q + N_{\text{img}}$  tokens, where each token has a hidden dimension  $D$ , and the per-head dimension is  $d$ , satisfying  $D = hd$ .

**Linear attention.** The computation of the per-token output  $O_i^{(d)}$  for linear attention with division-based normalization can be expressed as:

$$O_i^{(d)} = \frac{\phi(Q_i) \left( \sum_{j=1}^N \phi(K_j)^\top V_j \right)}{\phi(Q_i) \left( \sum_{m=1}^N \phi(K_m)^\top \right)}, \quad (8)$$

Theoretically, for the numerator, we have:

$$\underbrace{\phi(Q_i)}_{\mathbb{R}^{1 \times d}} \left( \sum_{j=1}^N \underbrace{\phi(K_j)^\top}_{\mathbb{R}^{d \times 1}} \underbrace{V_j}_{\mathbb{R}^{1 \times d}} \right) \longrightarrow \mathbb{R}^{1 \times d}, \quad (9)$$

where, first, a  $d \times 1$  matrix is multiplied by a  $1 \times d$  matrix, which costs  $\mathcal{O}(d^2)$ . Then, a  $1 \times d$  matrix is multiplied by an a  $d \times d$  matrix, which also costs  $\mathcal{O}(d^2)$ .

For the denominator, we have:

$$\underbrace{\phi(Q_i)}_{\mathbb{R}^{1 \times d}} \left( \sum_{m=1}^N \underbrace{\phi(K_m)^\top}_{\mathbb{R}^{d \times 1}} \right) \longrightarrow \mathbb{R}^{1 \times 1}, \quad (10)$$

where, a  $1 \times d$  matrix is multiplied by a  $d \times 1$  matrix, which costs  $\mathcal{O}(d)$ , which is negligible in the big- $\mathcal{O}$  sense.

Computing the final output  $O_i^{(a)}$  also costs  $\mathcal{O}(d)$ , which is negligible in the big- $\mathcal{O}$  sense. Thus, the per-token complexity is at most  $\mathcal{C}_{la,t} = 2d^2 = \mathcal{O}(d^2)$ .

For a single attention head processing  $N$  tokens, the total cost is at most:

$$\text{Linear attention, per-head: } \mathcal{C}_{la,h} = N\mathcal{C}_{la,t} = \mathcal{O}(Nd^2). \quad (11)$$

For the whole linear attention with  $h$  heads (and hidden dimension  $D = hd$ ), the total cost is:

$$\text{Linear attention: } \mathcal{C}_{la} = h\mathcal{C}_{la,h} = \mathcal{O}(NDd). \quad (12)$$

**Depthwise convolution.** The DWC module applies a  $k \times k$  depthwise convolution to  $N_{\text{img}}$  image tokens only, with a cost of:

$$\text{DWC module: } \mathcal{C}_{dwc} = \mathcal{O}(N_{\text{img}}Dk^2). \quad (13)$$

The ratio between the computational cost of the *DWC module* and that of *linear attention* is:

$$\frac{\mathcal{O}(N_{\text{img}}Dk^2)}{\mathcal{O}(NDd)} \leq \frac{k^2}{d}. \quad (14)$$

Note that the DWC module processes only  $N_{\text{img}}$  image tokens, while the linear attention processes both  $N_q$  query tokens and  $N_{\text{img}}$  image tokens ( $N = N_q + N_{\text{img}}$ ).

For our text-to-image model LINA-H, we have  $D = 1536$  and  $h = 16$ , so the per-head dimension is  $d = 96$ . Therefore, we obtain  $k^2/d = 0.26$ .

Note that the actual cost ratio is **smaller** than 0.26. The reasons are as follows. In LINA, the DWC module is applied only in the *decoder* blocks, which account for merely  $\frac{1}{3}$  of the total network depth. As a result, the additional computational overhead introduced by DWC is non-dominant.

**KV gate.** The KV gate  $g^{(k)}, g^{(v)} \in \mathbb{R}^{N_{\text{img}}}$  uses learnable parameters to scale the keys and values on a per-token basis.

$$\tilde{K}_j = \underbrace{g_j^{(k)}}_{\mathbb{R}^{1 \times 1}} \underbrace{\phi(K_j)}_{\mathbb{R}^{1 \times d}}, \quad \tilde{V}_j = \underbrace{g_j^{(v)}}_{\mathbb{R}^{1 \times 1}} \underbrace{V_j}_{\mathbb{R}^{1 \times d}}, \quad (15)$$

For a single head processing  $N_{\text{img}}$  tokens, the cost is at most:

$$\text{KV gate, per-head: } \mathcal{C}_{kvg,h} = 2N_{\text{img}}d = \mathcal{O}(N_{\text{img}}d). \quad (16)$$

For the whole linear attention with  $h$  heads (and hidden dimension  $D = hd$ ), the total cost is:

$$\text{KV gate: } \mathcal{C}_{kvg} = h\mathcal{C}_{kvg,h} = \mathcal{O}(N_{\text{img}}D). \quad (17)$$

The ratio between the computational cost of the *KV gate* and that of *linear attention* is:

$$\frac{\mathcal{O}(N_{\text{img}}D)}{\mathcal{O}(NDd)} \leq \frac{1}{d}. \quad (18)$$

Note that the KV gate processes only  $N_{\text{img}}$  image tokens, while the linear attention processes both  $N_q$  query tokens and  $N_{\text{img}}$  image tokens ( $N = N_q + N_{\text{img}}$ ).

Since the per-head dimension is  $d = 96$ , the additional computational cost introduced by the KV gate is negligible.

**Comparison to softmax attention.** The computational complexity of standard softmax attention is  $\mathcal{C}_{fa} = O(N^2D)$ , and the ratio between linear attention and softmax attention is:

$$\frac{\mathcal{C}_{la}}{\mathcal{C}_{fa}} = \frac{\mathcal{O}(NDd)}{\mathcal{O}(N^2D)} = \frac{d}{N}. \quad (19)$$

Note that when LINA operates at 1024px, we have  $N = 5120$ ,  $D = 1536$ , and  $h = 16$ , so  $d = D/h = 96$ . This gives a complexity ratio of  $d/N = 96/5120 \approx 0.019$ . Therefore, linear attention achieves a substantial reduction in computational cost, which is consistent with our measured FLOPs.

## F. How Our Findings Relate to Prior Work on Linear Attention

We note that neither the normalization types used in linear attention nor the locality augmentation techniques are our original inventions. However, to the best of our knowledge, our work is the *first* to systematically investigate these components in the context of *autoregressive image generation*. Prior studies such as Flattened Transformer (Han et al., 2023) and InLine (Han et al., 2024) only explored them in perception tasks such as image classification.

To clarify the relationship between our findings and existing results in other domains, we summarize the key similarities and differences below.

**Differences from visual perception tasks.** In autoregressive image generation, our results show that *division-based normalization* yields better *scaling behavior* for linear attention than subtraction-based normalization. This observation is not fully aligned with the conclusions drawn from perception tasks (e.g., InLine). We suspect that this discrepancy may arise from the inherent gap between generation and perception tasks. Issues such as “semantic confusion”, highlighted by InLine, may not be the main bottleneck in generative models. Instead, division-based normalization might be inherently more suitable for denoising-based generative processes. We admit that we do not yet have a theoretical explanation for this phenomenon. Nonetheless, we believe that the empirical results and the new data points we provide will be valuable for guiding future work.

**Similarities to visual perception tasks.** Consistent with findings in perception tasks (e.g., Flattened Transformer), our autoregressive generation results confirm that *linear attention indeed benefits from additional locality modeling*. This can be seen in the scaling behavior in Fig. 4-(a) in the main paper. Nevertheless, our work further raises two conceptual questions in Sec. 4, i.e., 1) Whether the softmax operation is the key reason behind the locality gap between softmax attention and linear attention; and 2) Whether locality modeling universally helps autoregressive image generation. Although our conclusions overlap with prior work in image classification, we believe these discussions offer useful conceptual insights into the role of locality in linear attention for autoregressive generation.

In summary, our results suggest that *linear attention in autoregressive image generation comes with task-specific considerations*, such as preferring division-based normalization, rather than directly inheriting conclusions from perception tasks. We hope our study can provide reliable guidelines for future research, helping to avoid large amounts of repetitive ablations.

## G. Scaling Behavior: Detailed Results

In Tab. 8, we present detailed results, as discussed in Sec. 4, comparing the scaling behavior of the four linear attention design choices. For evaluation metrics, we literally reported include FID-50K (Heusel et al., 2017), sFID (Nash et al., 2021), Inception Score (Salimans et al., 2016), and Precision/Recall (Kynkänniemi et al., 2019).

Table 8. Scaling performance of different linear attention design choices. We report the results on the class-conditional image generation using the ImageNet benchmark at  $256 \times 256$  resolution.

Linear Attention Setting	FID $\downarrow$ (w/o cfg)	sFID $\downarrow$	IS $\uparrow$	Precision $\uparrow$	Recall $\uparrow$
<i>Large (L):</i>					
Division-based Normalization, w/o DWC	13.13	7.58	105.26	0.65	0.61
Subtraction-based Normalization, w/o DWC	15.81	8.95	90.47	0.62	0.60
Division-based Normalization, w/ DWC	9.11	5.89	117.40	0.69	0.61
Subtraction-based Normalization, w/ DWC	9.02	5.77	116.54	0.70	0.61
<i>Extra Large (XL):</i>					
Division-based Normalization, w/o DWC	9.73	6.46	121.68	0.68	0.60
Subtraction-based Normalization, w/o DWC	12.10	7.50	107.07	0.66	0.60
Division-based Normalization, w/ DWC	7.25	5.17	127.93	0.71	0.61
Subtraction-based Normalization, w/ DWC	7.48	5.38	125.80	0.72	0.60
<i>Huge (H):</i>					
Division-based Normalization, w/o DWC	9.87	6.05	115.64	0.69	0.58
Subtraction-based Normalization, w/o DWC	11.10	7.08	107.25	0.67	0.59
Division-based Normalization, w/ DWC	6.53	5.01	130.31	0.72	0.60
Subtraction-based Normalization, w/ DWC	7.88	5.28	117.26	0.72	0.58

Table 9. Training setting of our text-to-image generation LINA.

Training Setting	Stage 1	Stage 2	Stage 3
Training Iterations	565K	600K	50K
Dataset Size	28M	28M	16M
Resolution	256px	512px	1024px
Base Learning Rate	$2e^{-4}$	$1e^{-4}$	$5e^{-5}$
Batch Size	$16 \times 48$	$4 \times 48$	$1 \times 48$
Weight Decay	0.02	0.02	0.02
Warm-up Steps	10000	10000	10000
Model EMA	0.99	0.99	0.99

## H. Detailed hyper-parameters on Text-to-image Generation

In Tab. 9, we present the training setting for the text-to-image generation experiments in Sec. 6, including the dataset size, batch size, learning rate, *etc.*. The training process can be divided into three stages. Our training is conducted using 48 NVIDIA A100 (40G) GPUs.

## I. KV Gate

### I.1. Ablation of KV gate Designs

The variants of the KV gate ablation are listed below.

#### Mode 1 (KV gate).

$$\begin{aligned}
 \tilde{K}_j &= g_j^{(k)} \phi(K_j), \quad \tilde{V}_j = g_j^{(v)} V_j, \quad \text{for } j \in [1, N] \\
 M &= \sum_{j=1}^N \tilde{K}_j^\top \tilde{V}_j = \sum_{j=1}^N g_j^{(k)} g_j^{(v)} M_j, \quad z = \sum_{m=1}^N \tilde{K}_m^\top, \quad O_i^{(\text{a})} = \frac{\phi(Q_i) M}{\phi(Q_i) z}.
 \end{aligned} \tag{20}$$

where  $g^{(k)}, g^{(v)} \in \mathbb{R}^N$  are learnable parameters.

**Mode 2 (K gate).**

$$\begin{aligned} \tilde{K}_j &= g_j^{(k)} \phi(K_j), \text{ for } j \in [1, N] \\ M &= \sum_{j=1}^N \tilde{K}_j^\top V_j = \sum_{j=1}^N g_j^{(k)} M_j, \quad z = \sum_{m=1}^N \tilde{K}_m^\top, \quad O_i^{(d)} = \frac{\phi(Q_i)M}{\phi(Q_i)z}. \end{aligned} \quad (21)$$

where  $g^{(k)} \in \mathbb{R}^N$  are learnable parameters.

**Mode 3 (V gate).**

$$\begin{aligned} \tilde{V}_j &= g_j^{(v)} V_j, \text{ for } j \in [1, N] \\ M &= \sum_{j=1}^N \phi(K_j)^\top \tilde{V}_j = \sum_{j=1}^N g_j^{(v)} M_j, \quad z = \sum_{m=1}^N \phi(K_m)^\top, \quad O_i^{(d)} = \frac{\phi(Q_i)M}{\phi(Q_i)z}. \end{aligned} \quad (22)$$

where  $g^{(v)} \in \mathbb{R}^N$  are learnable parameters.

**Mode 4 (KV gate + extra z gate).**

$$\begin{aligned} \tilde{K}_j &= g_j^{(k)} \phi(K_j), \quad \bar{K}_j = g_j^{(n)} \phi(K_j), \quad \tilde{V}_j = g_j^{(v)} V_j, \text{ for } j \in [1, N] \\ M &= \sum_{j=1}^N \tilde{K}_j^\top \tilde{V}_j = \sum_{j=1}^N g_j^{(k)} g_j^{(v)} M_j, \quad z = \sum_{m=1}^N \bar{K}_m^\top, \quad O_i^{(d)} = \frac{\phi(Q_i)M}{\phi(Q_i)z}. \end{aligned} \quad (23)$$

where  $g^{(k)}, g^{(v)}, g^{(n)} \in \mathbb{R}^N$  are learnable parameters.

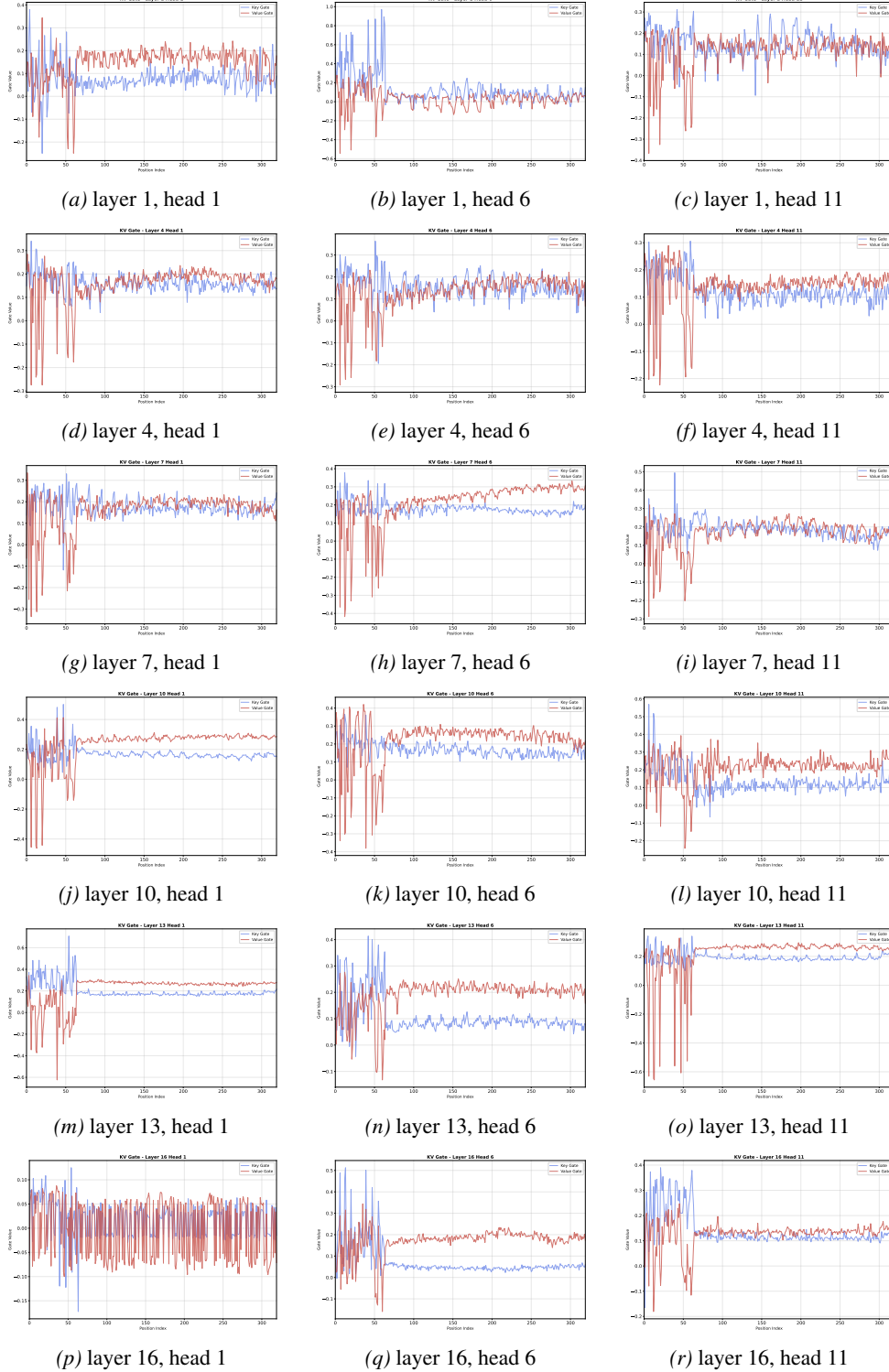
## I.2. Visualization

Figure 7 presents detailed visualizations of the learned KV gate values across different layers and heads. From the visualizations, we find a common pattern across layers and heads: the first 64 query tokens show fluctuations, while the following 256 image tokens remain relatively stable with distinct behaviors. We leave the analysis of text tokens to future work and focus here on the KV gate patterns for image tokens.

Our observations are three-folds: (1) From a cross-layer perspective, the KV gate patterns for image tokens also differ by layer. For example, in layer 1, head 1 the fluctuations are more pronounced, indicating substantial variation in KV gate values across image tokens. In contrast, in layer 13, head 1 the fluctuations are much weaker, suggesting that the values remain relatively stable across tokens. (2) From the perspective of value ranges, in many layers the KV gate values lie mostly within  $(-1, 1)$ , such as layer 10, head 6, layer 4, head 1, and layer 4, head 11. This suggests that, in certain cases, the model applies token-wise attenuation to both  $M$  and  $z$  when regulating memory in linear attention. (3) From the perspective of heads, the KV gate within the same layer seems to exhibit diverse patterns across different heads. For example, in layer 16, the fluctuations of head 6 and head 11 seems relatively stable, whereas head 1 seems to oscillate more strongly.

## J. More Qualitative Results

As illustrated in Fig. 8 and 9, we provide additional qualitative results sampled from 1024px images generated by LINA. LINA produces high-fidelity images with convincing details and textures. These results support our belief that the proposed LINA offers both practical effectiveness and potential value for generative modeling.



**Figure 7. KV gate visualization.** We plot the KV gate results for layers 1, 4, 7, 10, 13, 16 (indexed 1–16) and heads 1, 6, 11 (indexed 0–15). Across different layers and heads, the KV gate learns distinct patterns, allowing flexible memory management. Zoom in for best view.



Figure 8. Detailed qualitative results: 1024px samples from LINA, Part 1.

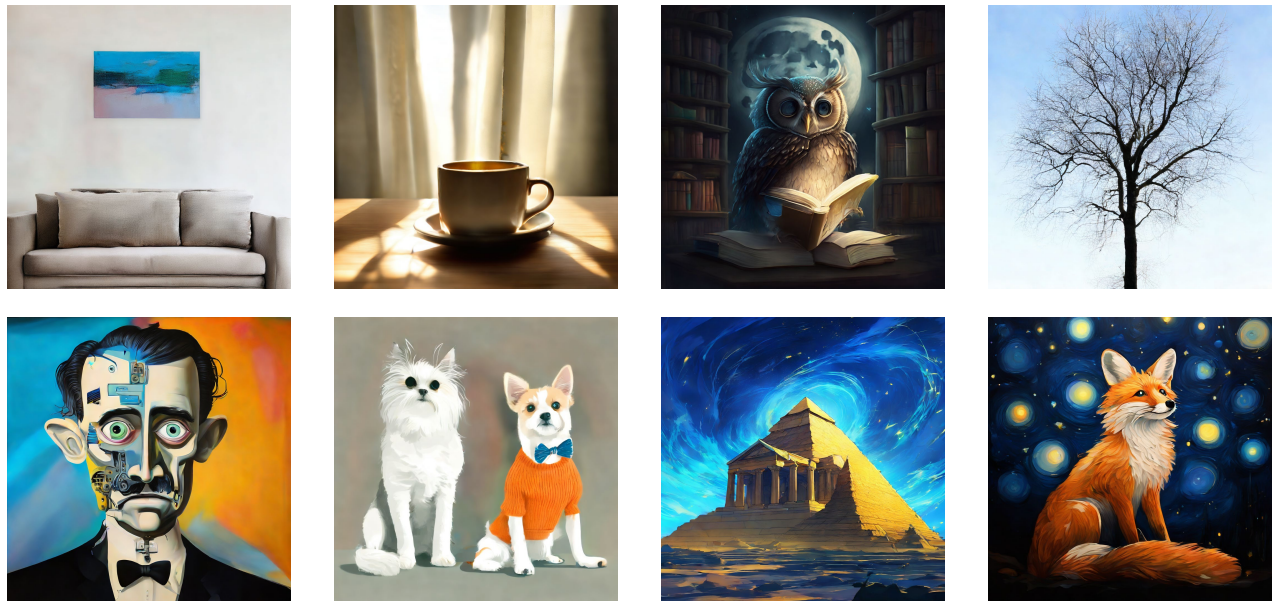


Figure 9. Detailed qualitative results: 1024px samples from LINA, Part 2.